Int J Adv Manuf Technol (2001) 17:489–497

The International Journal of
Advanced
Manufacturing
Technology

Efficient Chip Breaker Design by Predicting the Chip Breaking Performance

J. P. Choi and S. J. Lee

Department of Mechanical Engineering, Yonsei University, Seoul, Korea

As machining technology develops toward the unmanned and automated system, the need for chip control is considered increasingly important, especially in continuous machining such as in the turning operation. In this study, a systematic chip breaking prediction method is proposed using a 3D cutting model with the equivalent parameter concept. To verify the model, four inserts with different chip breaker parameters were tested and their chip breaking areas were compared with those obtained from the model. Finally, a new type insert (MF1) for medium-finish operations with variable parameters was designed by modifying the commercial one. The chip breaking region predicted by using the modified 3D cutting model for the above insert agrees with the one obtained experimentally. The newly designed insert showed better chip breaking ability than the base model, and other performance tests such as surface roughness, cutting force and tool wear also showed good results.

Keywords: Chip breaker; Chip control; Cutting Model; Insert; Turning

1. Introduction

Chip control is a major problem to be solved in automated machining systems. It involves a total system to produce chips that can be evacuated easily and reliably from the working zone and can be disposed of efficiently [1]. In general, uncontrolled chips are apt to cause poor surface quality, damage cutting tools and workpieces, and in serious cases, harm operators owing to tangled chips. So far, many attempts have been made to achieve desirable chips which are broken periodically.

Arsecularatne and Fowle [2] calculated the chip flow direction from the tool geometry and cutting conditions in a turning operation, and predicted cutting forces and the surface roughness of the machined surface on the basis of the equivalent parameter concept. Rahman and Zhang [3] suggested a systematic method to predict chip breakage of triangular inserts using similar equivalent parameters. Nedeβ and Hintze [4] modelled the chip formation process for various type of inserts and tried to establish the variables related to chip control. Prior to the above works, Spaans [5] studied the fundamental mechanism of 3D chip-curling, chip breaking and chip control.

While these workers showed their interest in modelling the cutting process, some others made an effort to detect chip forms or chip breakage more efficiently and to improve the chip breaking ability. For example, Andreasen and de Chiffre [6] analysed the spectrum of feed force to find out the chip breakage frequency, and Ding [7] improved the breakability of AISI1008 chips by lowering the chip temperature to its embrittlement temperature using liquid nitrogen (LN2). Grzesik [8] adopted specific cutting energy to identify chip forms and suggested that there is some distinguishable uniformity in the distribution of the total cutting energy for finish, medium, and rough machining operations. Nedeβ [9] monitored chip forms in real-time using the acoustic emission signals.

Nowadays, there are hundreds of cutting tools available with various chip breaker geometries. However, tool design depends largely on the experience of the designers and, furthermore, "try and see" methods are still popular because of the lack of a full understanding of the basic chip formation mechanism and of the difficulties in systematically predicting chip breakage. Since such a method is time-consuming and requires considerable funds, it is very ineffective. Moreover, we cannot establish the performance of the tool at the design stage.

In this study, whether chips produced under various cutting conditions break or not is predicted by accepting and modifying the equivalent parameter concept suggested by several researchers. To verify the model, four inserts with different chip breaker parameters were made and tested. Experimental results showed that the cutting model can satisfactorily predict the chip breakability. Finally, a new insert that has variable parameters along the main cutting edge was designed by changing the parameters of the commercial one to enhance the chip breakability based on the simulation. The newly designed insert showed a broader chip breaking area than the base model, and other performance tests such as surface roughness, cutting force, and tool wear also showed good results.

Correspondence and offprint requests to: J. P. Choi, Department of Mechanical Engineering, Yonsei University, 134 Shinchon-dong, Seodaemun-gu, Seoul, Korea. E-mail: feel2@shinbiro.com

2. Cutting Model for a Grooved Chip Breaker

In order to predict the chip breakage systematically, the equivalent parameter concept suggested by several researchers [2–4] was used. First, the chip flow angle was calculated, and all variables were redefined along and perpendicular to the chip flow direction. The advantage of using equivalent parameters is that they can simplify a complicated 3D cutting process to a 2D cutting process.

The cutting model presented in the following sections is confined to a rhombus type insert which has an included angle of 80° and a grooved chip breaker, but it can be applied to other types of inserts having variable chip breaker parameters.

2.1 Chip Side-Flow Angle

Because equivalent parameters are defined according to the chip side-flow direction (or chip flow angle) as mentioned above, the exact prediction of the chip flow angle is very important. So far, there have been many papers which calculate the chip flow angle from various viewpoints. Here, the model of Colwell is employed because it is the simplest and most appropriate. The chip flow angle (η_c) can be calculated easily from the geometric relation between the tool geometry and the cutting condition. It is a function of the nose radius (r), depth of cut (d), feedrate (f), and side cutting edge angle (C_s) and is defined differently according to the depth of cut.

$$\eta_c = \tan^{-1}\left(\frac{\sqrt{(2rd - d^2)} + f/2}{d}\right) \qquad (d < r) \tag{1}$$

$$\eta_c = \tan^{-1}\left(\frac{r - (d - r)\tan C_s + f/2}{d}\right) \ (d \geq r) \tag{2}$$

2.2 Definition of Equivalent Parameters [3]

The definition of equivalent parameters suggested in [3] is adapted, and some modifications are made to complement the existing model. As shown in Fig. 1, the equivalent cut width (w_{ce}) is measured perpendicular to the chip flow direction, which is the width linking two extreme points of the undeformed cut section. The equivalent cut thickness (t_{ce}) is measured along the chip flow direction, namely,

$$w_{ce} = \frac{d}{\cos \eta_c} \tag{3}$$

$$t_{ce} = \frac{1}{w_{ce}} \int t_c \mathrm{d}w_{ce} = \frac{A_t}{w_{ce}} \tag{4}$$

Equation (4) shows that the mean cut thickness is used as the equivalent cut thickness.

All other variables such as land width (L), groove width (W) and land angles (α_1, α_2) can be defined in a similar way using the equivalent parameter concept. The equivalent land width (L_e) is defined as the mean land width, i.e. equal to the area of the land width within the undeformed cut section (A_L) divided by the equivalent cut width (w_{ce}). The groove width along the chip flow direction is considered as the equivalent groove width (W_e). The equivalent parameters of primary (α_{1e}) and secondary (α_{2e}) land angles can be obtained by coordinate transformation of the normal vectors of the land face on the main cutting edge and on the tool corner (see [3]). Figure 2 shows a cross-sectional view of the chip breaker.

The chip backflow angle (η_b) is considered very important because it is the angle at which the chip enters the groove, and it is related to the chip curl radius. Its equivalent parameter (η_{be}) can be expressed in a similar way. By introducing equivalent parameters and re-writing, η_{be} has a lower limit of α_{1e} and an upper limit of α_{2e}.

$$\alpha_{1e} \leq \eta_{be} \leq \alpha_{2e} \tag{5}$$

In general, η_{be} is known to be a function of the ratio of feedrate to land width (f/L), side rake angle and land angles. Unfortunately, there is no theoretical relationship between the chip backflow angle and its influencing factors. In this study, by combining the models in [3] and [4], a new relation that has the lower and upper limits of Eq. (5) is proposed.

$$\eta_{ee} = \alpha_{2e} - (\alpha_{2e} - \alpha_{1e}) \exp(-k(t_{ce}/L_e)) \tag{6}$$

k is a constant determined from the workpiece material.

The equivalent curl radius (R_e) can be calculated easily using the relationship between the equivalent groove width (W_e), the

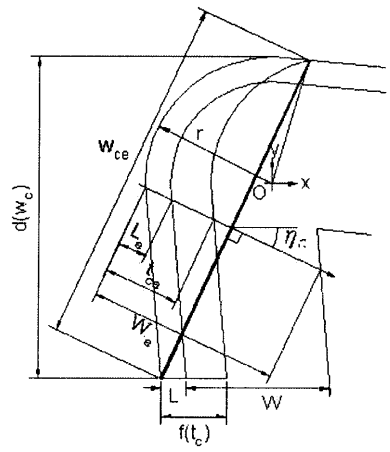

Fig. 1. Definition of equivalent parameters.

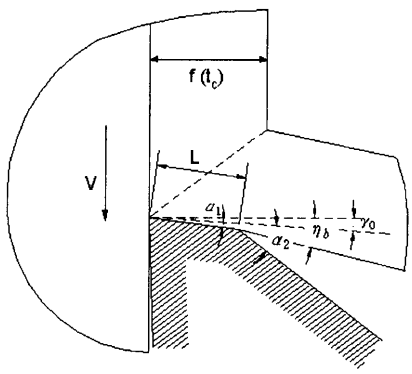

Fig. 2. The cross-sectional view of the chip breaker.

equivalent chip backflow angle (η_{ee}), and the backwall height (h), as depicted in Fig. 3.

$$R_e = \frac{W_e \sec\theta}{2\sin(\eta_{ee} + \theta)} \quad \left(\theta = \tan^{-1}\left(\frac{h}{W_e}\right)\right) \tag{7}$$

2.3 Chip Breaking Criterion

The chip strain ratio (n) is used as a chip breaking criterion. First, the tensile strain of chips (ϵ_{chip}) is a function of the chip thickness and chip curl radius. Introducing the equivalent parameter concept, it can be simply expressed as shown in Eq. (8).

$$\epsilon_{chip} = \frac{t_{che}}{2R_e}\left(1 - \frac{1}{C}\right) \tag{8}$$

Here, t_{che} is the equivalent chip thickness which mainly depends on the feedrate and depth of cut. C is a ratio between the chip radius at fracture (R_f) and the equivalent chip radius leaving the groove (R_e). Finally, the chip strain ration (n) is defined as follows.

$$n = \frac{\epsilon_{chip}}{\epsilon_f} \tag{9}$$

It can be inferred that if the chip strain is greater than the chip fracture strain, the chip will break.

3. Simulation and Verification Experiment

3.1 Simulation of Equivalent Parameters

Some simulations to verify the above cutting model are described for a medium cutting insert with constant parameters such as land width, groove width, land angle, and backwall height, as shown in Table 1. The workpiece used in the simulation and the experiment is mild steel, SCM440.

Figure 4 shows some of the simulation results for an insert with constant chip breaker parameters. In Fig. 4(*a*), the equivalent land width is nearly uniform at a relatively large depth of cut, while it decreases dramatically with smaller depths of cut. The feedrate, however, has only negligible effect on the equivalent land width. Figure 4(*b*) shows that at low feedrates and depths of cut, the equivalent groove width becomes so large that chips have a large up-curl radius, as shown in Fig. 4(*c*). That is, the chip breaking ability is enhanced at high feedrates and depths of cut because, in general, the large chip curl radius involves a small value of chip strain.

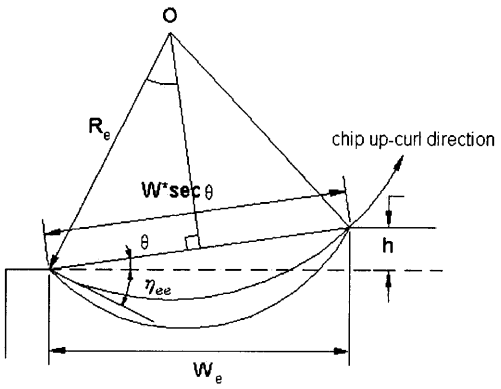

Fig. 3. Chip curl radius considering the backwall height.

Table 1. Specification of chip breaker and tool holder used in the simulation.

	Chip breaker parameters	Value
Chip breaker CNMG120408-B25	r	0.8 mm
	L	0.25 mm
	W	1.65 mm
	α_1	0°
	α_2	14°
	h	0.05 mm
Tool holder PCLNR2525-M12	C_s	95°
	i	5°
	γ_0	–5°

3.2 Verification Experiment

To ascertain the chip breaking region, cutting experiments were performed using the B25 type insert used in the simulation and other inserts (X141, X137) with different chip breaker parameters. Applying the cutting model for each insert, the chip breaking region is predicted. Sample chips are collected from experiments under various cutting conditions, and a real chip map is obtained. Then, the validity of the cutting model is verified by comparing the two regions. Chip breaker parameters used in the experiments are nose radius, land width, and groove width, and are listed in Table 2. Land angles and backwall height are fixed, i.e. $\alpha_1 = 0°$, $\alpha_2 = 14°$ and $h = 0.05$ mm. The same tool-holder and constant cutting velocity $V = 180$ m min^{-1} are used.

Figures 5, 6, and 7 compare chip breaking regions obtained from the simulation and from the cutting experiments for each insert described in Table 2. Chip breaking diagrams from the simulation are shown on the lefthand side of each figure, and chip maps obtained from the experiment are shown on the righthand side. Feedrate increases from 0.05 mm rev^{-1} to 0.40 mm rev^{-1} with an interval of 0.05 mm rev^{-1} and are shown on the abscissa. Depth of cut increases from 0.5 mm to 4.0 mm with each step of 0.5 mm. From the figures, as feedrate and depth of cut decrease, tangled chips with large curl radius are produced, which means that chips must be controlled properly.

In Figs 5(*a*), 6(*a*), and 7(*a*), the numbers indicate the chip strain ratio calculated from the model, as defined in Eq. (9). The area surrounded by heavy lines is the chip breaking region predicted from the model. The shaded cells of each table shows that the broken chips are obtained under the corresponding cutting conditions.

There are some differences between the predicted chip breaking region and the experimentally obtained region. However,

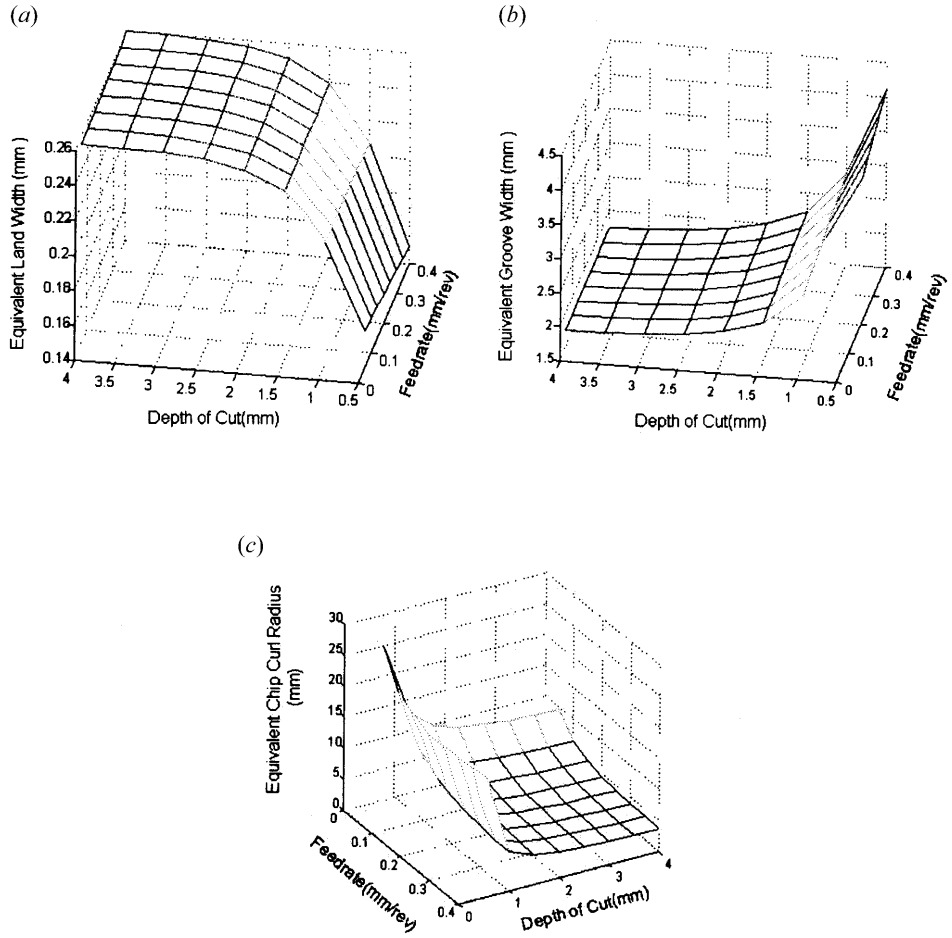

Fig. 4. Simulation for the B25 insert with constant chip breaker parameters. (*a*) The equivalent land width. (*b*) The equivalent groove width. (*c*) The equivalent chip curl radius.

Table 2. Chip breaker parameters used in experiments.

	B25 (mm)	X141 (mm)	X137 (mm)
Nose radius (*r*)	0.8	0.4	1.2
Land width (*L*)	0.25	0.15	0.25
Groove width (*W*)	1.65	1.3	1.6

in the case of the B25 type insert (Fig. 5), two results correspond well, except for 3 out of 64 points in total. Only 2 points for the X141 (Fig. 6) and 4 points for the X137 (Fig. 7) show different results. Therefore, it can be concluded that the proposed cutting model reliably predicts the chip breakage, even though it uses simplified variables and relationships. It can be applied to choose the proper chip breaker parameters to improve the chip breaking ability when designing a new insert. This is explained in the next section.

4. Chip Breaker Design with Variable Parameters

In the previous sections, a systematic approach for predicting the chip breakage was presented briefly, and some experiments to verify the model were performed. Comparing chip maps from experiments with chip breaking diagrams from the suggested model, it can be seen that the cutting model reliably predicts whether chip breakage will occur.

In order to expand the availability of the model, a new type insert with variable chip breaker parameters is designed by using simulated effects of chip breaker parameters on the chip breakability, and modifying the existing insert. The commercial B25 type insert used in the simulation and the experiments shows poor chip breaking ability, especially at low feedrates and depths of cut. To overcome this problem, a new type insert (MF1) is designed to perform well under light cutting conditions. Then, applying the previously stated model to the new insert, the chip breaking diagram is obtained. Furthermore, the chip map from the experiments is compared to the theoretical one. Finally, other performance tests such as surface roughness, cutting force, and tool wear are performed.

4.1 Effects of Chip Breaker Parameters on the Chip Breakability

Jawahir and Fang [10] showed how the chip breaker design parameters can be estimated for effective chip breaking at

(a)

depth of cut (mm) \ feedrate (mm/rev)	0,05	0,10	0,15	0,20	0,25	0,30	0,35	0,40
4,0	0,09	0,43	0,86	1,35	1,83	2,29	2,73	3,12
3,5	0,12	0,44	0,85	1,32	1,79	2,26	2,72	3,16
3,0	0,14	0,44	0,82	1,26	1,72	2,19	2,65	3,11
2,5	0,15	0,42	0,78	1,18	1,61	2,05	2,50	2,95
2,0	0,15	0,39	0,71	1,07	1,45	1,85	2,26	2,67
1,5	0,13	0,34	0,60	0,90	1,22	1,55	1,88	2,22
1,0	0,10	0,25	0,44	0,65	0,87	1,10	1,32	1,54
0,5	0,05	0,11	0,18	0,24	0,29	0,34	0,38	0,42

(b)

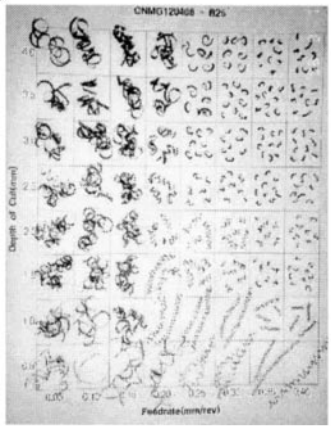

Fig. 5. Comparison of chip breaking regions obtained from the simulation and the experiment for the B25 type insert. (*a*) Chip breaking diagram of B25 type. (*b*) Chip map of B25 type.

(a)

depth of cut (mm) \ feedrate (mm/rev)	0,05	0,10	0,15	0,20	0,25	0,30	0,35	0,40
4,0	0,17	0,75	1,45	2,16	2,83	3,44	3,97	4,45
3,5	0,22	0,78	1,45	2,13	2,80	3,43	4,01	4,56
3,0	0,26	0,79	1,42	2,08	2,73	3,36	3,97	4,56
2,5	0,29	0,78	1,37	1,99	2,62	3,23	3,84	4,44
2,0	0,29	0,75	1,30	1,87	2,45	3,03	3,61	4,18
1,5	0,28	0,70	1,18	1,70	2,22	2,73	3,24	3,75
1,0	0,24	0,59	1,01	1,43	1,85	2,25	2,65	3,03
0,5	0,15	0,37	0,62	0,87	1,10	1,31	1,50	1,67

(b)

Fig. 6. Comparison of chip breaking regions obtained from the simulation and the experiment for the X141 type inserts. (*a*) Chip breaking diagram of X141 type. (*b*) Chip map of X141 type.

(a)

depth of cut (mm) \ feedrate (mm/rev)	0,05	0,10	0,15	0,20	0,25	0,30	0,35	0,40
4,0	0,09	0,41	0,83	1,30	1,77	2,23	2,65	3,04
3,5	0,11	0,42	0,81	1,25	1,71	2,17	2,61	3,04
3,0	0,13	0,41	0,77	1,18	1,61	2,05	2,49	2,93
2,5	0,14	0,38	0,70	1,07	1,46	1,87	2,29	2,71
2,0	0,13	0,34	0,61	0,92	1,26	1,61	1,98	2,34
1,5	0,10	0,27	0,48	0,72	0,98	1,25	1,53	1,81
1,0	0,08	0,18	0,31	0,44	0,58	0,71	0,84	0,97
0,5	0,05	0,11	0,17	0,22	0,27	0,31	0,35	0,38

(b)

Fig. 7. Comparison of chip breaking regions obtained from the simulation and the experiment for the X137 type insert. (*a*) Chip breaking diagram of X137 type. (*b*) Chip map of X137 type.

reduced power consumption. They analysed the chip breaking performance (e.g. the chip up-curl radius) from a series of well-designed machining experiments and tried to achieve the optimum parameters.

Here, effects of chip breaker parameters and cutting conditions on the chip breaking are summarised in Fig. 8. The variation of the chip curl radius and the chip strain directly related to the chip breaking is simulated by varying each parameter. It can be used as a basis for determining the parameters.

4.2 Selection of Chip Breaker Parameters and Design of a New Insert

From Fig. 8, each parameter is selected to enhance the chip breakability, and the Taguchi method is used to select the optimum parameters. The new insert is designed so that it breaks chips over a wider range, especially for light cutting conditions including the chip breaking range of the commercial B25 type insert.

First, the nose radius was 0.8 mm which is commonly used for the commercial medium-finish inserts. Since the small land width results in a large chip backflow angle and a small chip curl radius, chips break well even at low feedrates. However, a very small land width tends to have a weak cutting edge strength and causes chipping of the cutting tool. In this research, the land width is designed to vary linearly with depth of cut. Even though a small groove width makes the chip curl radius compact, chips cannot use the groove profile at high feedrates. Therefore, it needs a lower limit value and is designed to vary linearly along the main cutting edge as in the case of the land width. Large land angles increase the chip backflow angle (decrease of the chip curl radius) and decrease cutting forces owing to the reduced contact area between the insert and the chip produced. However, very large land angles make the tool so sharp that a catastrophic tool fracture may occur. In the case of the backwall height, an appropriate value must be selected considering both the chip curl radius and cutting forces.

Figure 9 shows the newly designed insert with selected parameters based on the previous concept. Some characteristic parameters are listed in Table 3.

4.3 Modelling and Simulation of the MF1 Insert

The B25 type insert has a constant land width and groove width along the cutting edge. On the other hand, the MF1 insert has a linearly varying land width and groove width along the main cutting edge and different land angles, as shown in Fig. 9, so, related equivalent parameters must be recalculated according to the geometry. However, the cut width and the cut thickness are the same as those for the B25 insert because they are determined from cutting conditions only.

The equivalent land width (L_e), the mean land width, is equal to the area of land width within the undeformed section divided by the equivalent cut width. Because the land width varies linearly along the cutting edge, it can be classified into (see Fig. 9 (*b*)):

case 1: $d \leq r$
case 2: $r < d \leq (r + a)$
case 3: $(r + a) \leq d$

Similarly, as the equivalent groove width (W_e) is defined as the groove width along the chip flow direction, it can also be classified into:

case 1: $d \leq r$
case 2: $r < d \leq (r + a)$
case 3: $(r + a) < d \leq (r + p)$
case 4: $(r + p) \leq d$

Figure 10 shows the simulation results for the equivalent land width, the equivalent groove width, and the equivalent chip curl radius for the MF1 insert. The equivalent land width of MF1 (Fig. 10(*a*)) decreases almost linearly with a smaller depth of cut. Since it shows much smaller values at low depths of cut when compared with that of B25 (Fig. 4(*a*)), it can be inferred that chip breaking may occur even at lower depths of cut. Figure 10(*b*) shows that the equivalent groove width of

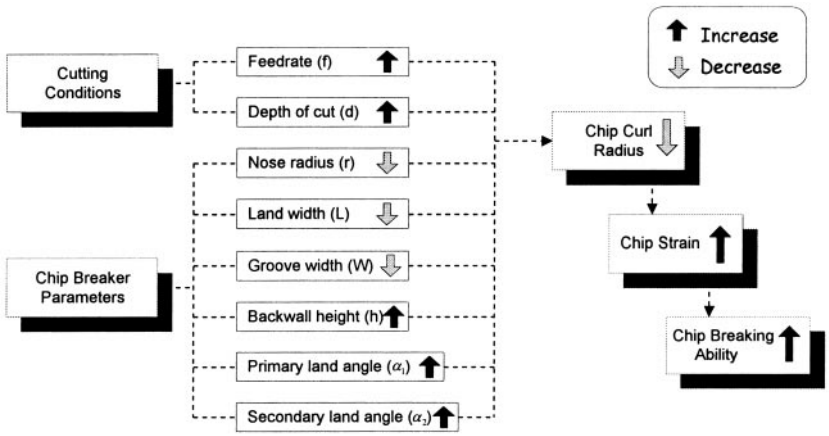

Fig. 8. Effects of cutting condition and chip breaker parameters on the chip breaking.

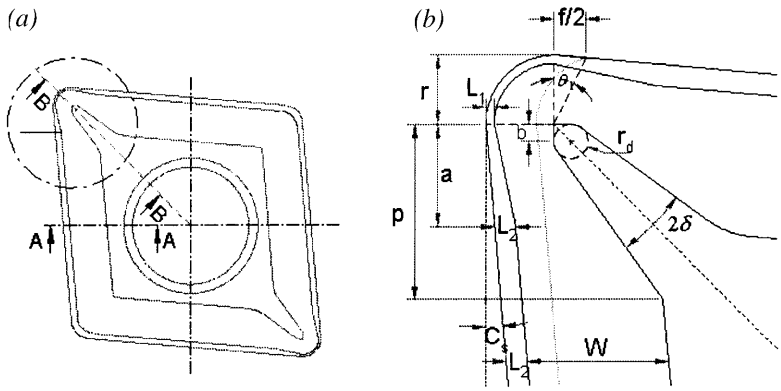

Fig. 9. The new insert (MF1) with variable parameters along the main cutting edge. (*a*) The newly designed insert (MF1). (*b*) Applying the cutting model to MF1.

Table 3. Dimension of the MF1 type chip breaker.

Parameter	r (mm)	L_1 (mm)	L_2 (mm)	W (mm)	h (mm)	α_1 (deg.)	α_2 (deg.)	a (mm)	b (mm)
Value	0.8	0.10	0.20	1.60	0.10	5	15	1.2	0.2

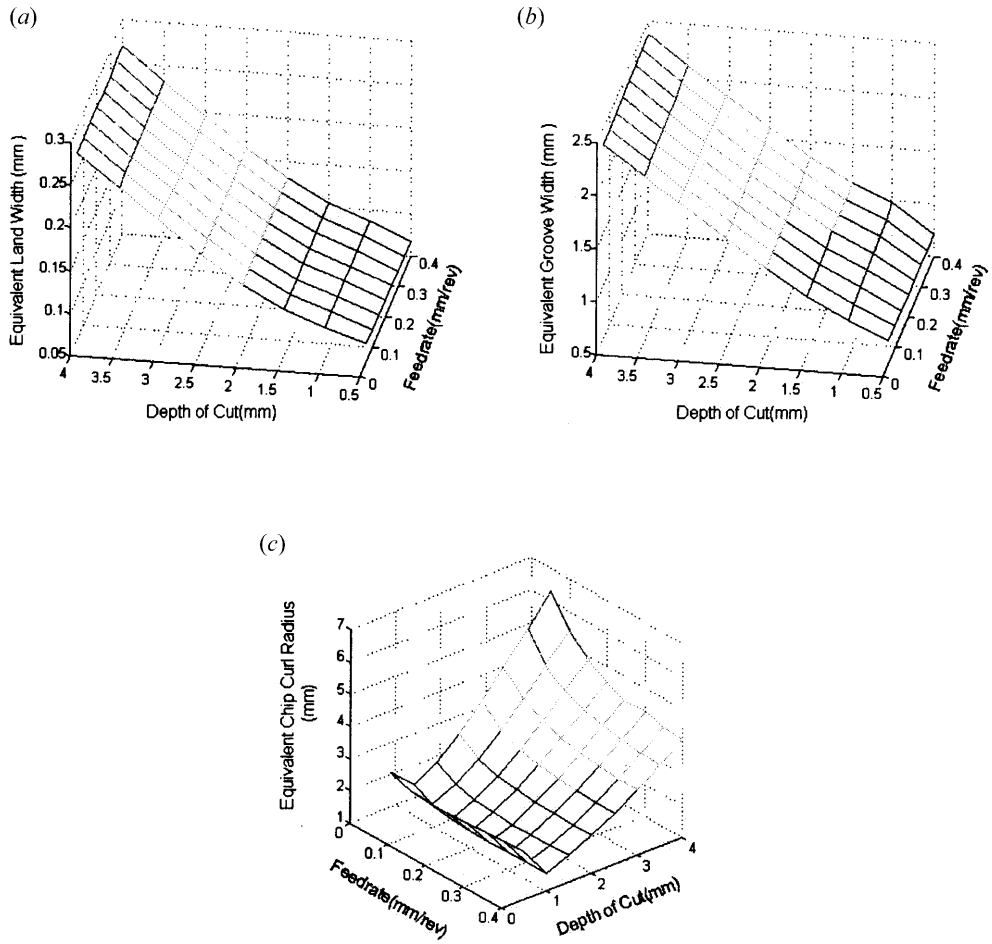

Fig. 10. Simulation for the MF1 insert with varying chip breaker parameters. (*a*) The equivalent land width. (*b*) The equivalent groove width. (*c*) The equivalent chip curl radius.

(a)

depth of cut (mm) \ Feedrate (mm/rev)	0,05	0,10	0,15	0,20	0,25	0,30	0,35	0,40
4,0	0,14	0,51	0,92	1,34	1,74	2,12	2,47	2,79
3,5	0,22	0,63	1,08	1,55	2,01	2,46	2,89	3,30
3,0	0,31	0,76	1,27	1,80	2,33	2,85	3,37	3,86
2,5	0,42	0,94	1,51	2,11	2,71	3,31	3,90	4,48
2,0	0,55	1,15	1,80	2,48	3,15	3,83	4,49	5,16
1,5	0,69	1,39	2,14	2,90	3,65	4,38	5,11	5,84
1,0	0,78	1,58	2,42	3,23	4,02	4,79	5,52	6,23
0,5	0,52	1,02	1,49	1,94	2,35	2,73	3,09	3,42

(b)

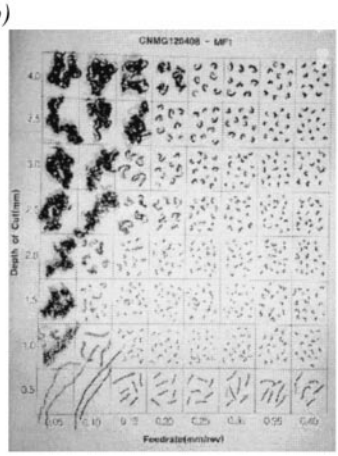

Fig. 11. Comparison of chip breaking regions obtained from the simulation and the experiment for the MF1 type insert. (*a*) Chip breaking diagram of MF1 type. (*b*) Chip map of MF1 type.

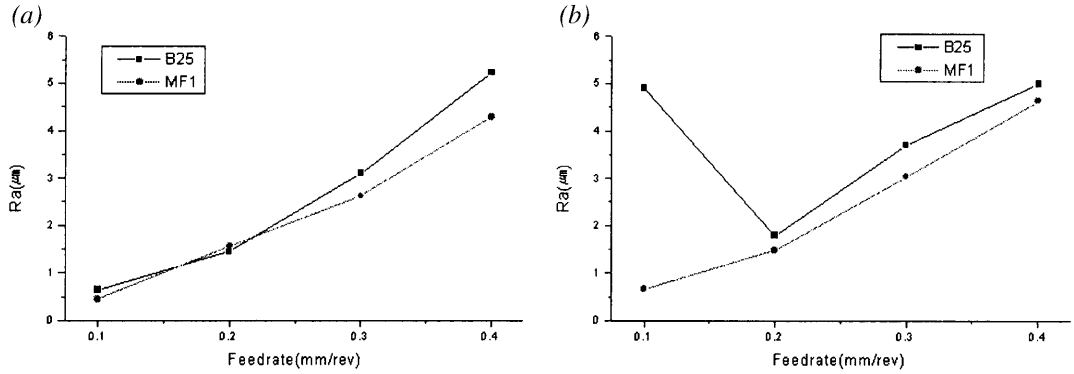

Fig. 12. The surface roughness test results (R_a). (*a*) d = 1 mm, (*b*) d = 3 mm.

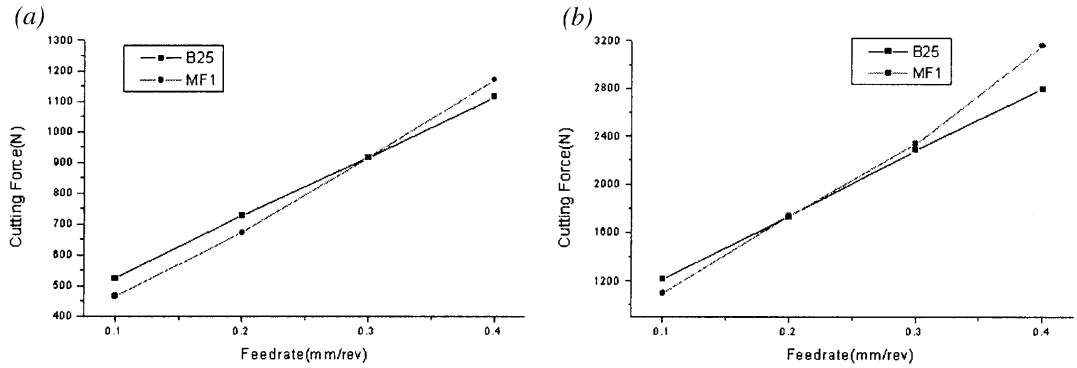

Fig. 13. Total cutting forces (N). (*a*) d = 1 mm, (*b*) d = 3 mm.

MF1 also decreases linearly as the depth of cut becomes smaller. Because the smaller groove width produces a smaller chip curl radius, MF1 makes the chip breaking easier than B25 (Fig. 4(*b*)). Finally, in Fig. 10(*c*), the equivalent chip curl radius of MF1 becomes much smaller than that of B25 (Fig. 4(*c*)), especially at low feedrates and low depths of cut. Since the smaller the chip curl radius, the larger the chip tensile strain, even in the case of small thicknesses, it can be predicted that the chip breaking ability will be enhanced, particularly at light cutting conditions.

4.4 Experiment and Performance Test

From the above simulation results, the newly designed MF1 with modified parameters has a more desirable performance in

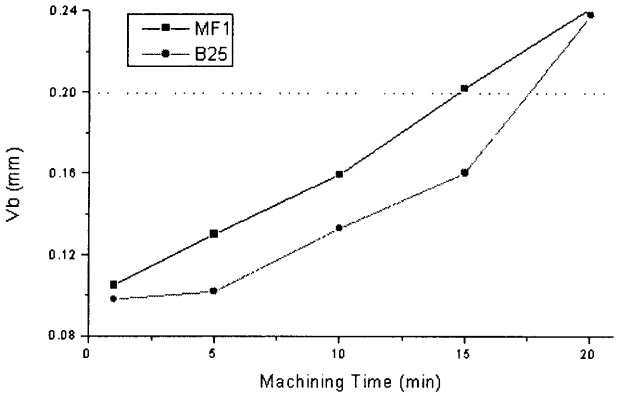

Fig. 14. Tool life – average flank wear.

breaking chips than the commercial B25 insert. In order to ascertain this fact, some experiments are performed in this section as before and other performance tests such as for surface roughness, cutting forces, and tool life are also executed.

Figure 11(*a*) shows a chip breaking diagram for the MF1 insert obtained from the simulation of the cutting model. As before, if the number of each cell is larger than 1, chips produced under that condition will be broken. The shaded areas mean that broken chips are actually produced (See Fig. 11(*b*)). When comparing Figs 11(*a*) and 11(*b*), simulation results agree well with experimental results, except in 2 out of 64 cases. It should be noted that simple changes of chip breaker parameters improve the chip breaking ability greatly.

Even though the chip breaking ability is a major problem in designing new inserts, other performance factors must also be satisfied. So, several tests such as surface roughness, cutting force, and the tool life are performed. The surface roughness at different depths of cut is plotted in Fig. 12 for the B25 and the MF1 insert. At d = 1.0 mm (small depth of cut) there is no significant difference between the two, but MF1 has a somewhat smaller value than B25 as the feedrate increases. At d = 3.0 mm (large depth of cut) the surface roughness of MF1 is smaller than that of B25 for all feedrates. At f = 0.1 mm rev^{-1}, the surface roughness of B25 is extraordinarily large because uncontrolled and entangled chips scratch the machined surface. Even though chips are not broken in the case of MF1 at the same feedrate, controlled and up-curled chips are produced and evacuated well away from the cutting zone without causing any damage to the workpiece.

Figure 13 shows the total cutting forces measured using a tool dynamometer. There are no significant differences in both cases, but it can be noted that cutting forces of B25 are larger at small feedrates and the cutting forces for MF1 are higher at larger feedrates. This is because the large land angles and the small land width of MF1 result in smaller cutting forces at small feedrates on the one hand, and the large backwall height of MF1 results in larger cutting forces at high feedrates on the other.

As a measure of tool life, the average flank wear is considered. Cutting conditions are fixed as follows: V = 180 m min^{-1}, d = 2.5 mm, f = 0.25 mm rev^{-1}. As seen in Fig. 14, the tool wear of MF1 progresses faster than that of B25 because the small land width and the large land angles of MF1 lead to a high cutting temperature and heat concentration at the cutting zone.

5. Conclusion

In this paper, a systematic approach is described for predicting the chip breaking with given chip breaker parameters and cutting conditions using the equivalent parameters concept, and some modification of the model is suggested. Cutting experiments are performed to verify the model and show a satisfactory correspondence between the predicted chip breaking region and the experimentally obtained chip map. Through simulation, the effects of each parameter on the chip breakage are examined. Using the simulation results, a new insert with variable parameters along the main cutting edge is designed and simulated. From the simulation and the verification experiments, it is shown that the new insert has a better chip breaking ability than the base model. Finally, some performance tests such as surface roughness, cutting forces, and tool life are performed. It can be seen that the performance of the new insert is better than or at least as good as the base model.

By predicting the chip breaking performance in the design stage, a reliable and systematic insert design can be achieved. This also considerably reduces the cost and time required.

References

1. S. Jawahir, “Recent development in chip control research and applications”, Annals CIRP, 42/2, pp. 659–685, 1993.
2. J. A. Arsecularatne and R. F. Fowle, “Prediction of chip flow direction, cutting forces and surface roughness in finish turning”, Journal of Manufacturing Science and Engineering, 120, pp. 1–12, 1998.
3. M. Rahman and X. D. Zhang, “A three dimensional model of chip flow, chip curl and chip breaking under the concept of equivalent parameters”, International Journal of Machine Tools and Manufacture, 35(7), pp. 1015–1031, 1995.
4. C. Nedeβ, W. Hintze, “Characteristic parameters of chip control in turning operations with indexable inserts and three-dimensionally shaped chip formers”, Annals CIRP, 38(1), pp. 75–79, 1989.
5. C. Spaans, “The fundamentals of three-dimensional chip curl, chip breaking and chip control”, PhD Paper, TH Delft, 1971.
6. J. L. Andreasen and L. De Chiffre, “Automatic chip-breaking detection in turning by frequency analysis of cutting force”, Annals CIRP, 42(1), pp. 45–48, 1993.
7. Y. Ding, “Improvement of chip breaking in machining low carbon steel by cryogenically precooling the workpiece”, Transactions ASME, 120, pp. 76–83, 1998.
8. W. Grzesik, “An energy approach to chip-breaking when machining with grooved tool inserts”, International Journal of Machine Tools and Manufacture, 37(5), pp. 569–577, 1997.
9. C. Nedeβ, “Real-time monitoring and controlling of chip form in turning processes with acoustic emission using thin film sensors”, Transactions NAMRI/SME, 14, pp. 99–104, 1996.
10. I. S. Jawahir and X. D. Fang, “A knowledge-based approach for desining effective grooved chip breakers – 2D and 3D chip flow, chip curl and chip breaking”, International Journal of Advanced Manufacturing Technology, 10, pp. 225–239, 1995.